

Benchmark performance of anodized vs. sandblasted implant surfaces in an acute dehiscence type defect animal model

Shakeel Shahdad^{1,2}  | Dieter Bosshardt³ | Mital Patel^{1,2} | Nahal Razaghi¹ | Anuya Patankar¹ | Mario Rocuzzo^{4,5,6} 

¹Barts Health NHS Trust, The Royal London Dental Hospital, London, UK

²Barts and The London School of Medicine and Dentistry, Queen Mary University of London, London, UK

³Department of Periodontology, University of Bern, Bern, Switzerland

⁴Private practice, Torino, Italy

⁵Department of Maxillo-facial Surgery, University of Torino, Torino, Italy

⁶Department of Periodontics and Oral Medicine, University of Michigan, Ann Arbor, Michigan, USA

Correspondence

Shakeel Shahdad, Department of restorative Dentistry, The Royal London Dental Hospital, Turner Street, E1 1DE, London, UK.

Email: s.shahdad@qmul.ac.uk

Funding information

Institut Straumann

Abstract

Objectives: Crestal bone formation represents a crucial aspect of the esthetic and biological success of dental implants. This controlled preclinical study analyzed the effect of implant surface and implant geometry on de novo crestal bone formation and osseointegration.

Materials and methods: Histological and histomorphometrical analysis was performed to compare three implant groups, that is, (1) a novel, commercially available, gradient anodized implant, (2) a custom-made geometric replica of implant “1,” displaying a superhydrophilic micro-rough large-grit sandblasted and acid-etched surface, and (3) a commercially available implant, having the same surface as “2” but a different implant geometry. The study applied a standardized buccal acute-type dehiscence model in minipigs with observation periods of 2 and 8 weeks of healing.

Results: The amount of newly formed crestal bone (BATA) around control groups (2) and (3) was significantly increased when compared to the test group (1) at the 8 weeks of healing time point. Similar results were obtained for all parameters related to osseointegration and direct bone apposition, to the implant surface (dBIC, VBC, and fBIC), demonstrating superior osseointegration of the moderately rough, compared to the gradient anodized functionalization. After 2 weeks, the osseointegration (nBIC) was found to be influenced by implant geometry with group (3) outperforming groups (1) and (2) on this parameter. At 8 weeks, nBIC was significantly higher for groups (2) and (3) compared to (1).

Conclusions: The extent (BATA) of de novo crestal bone formation in the acute-type dehiscence defects was primarily influenced by implant surface characteristics and their ability to promote osseointegration and direct bone apposition. Osseointegration (nBIC) of the apical part was found to be influenced by a combination of surface characteristics and implant geometry. For early healing, implant geometry may have a more pronounced effect on facilitating osseointegration, relative to the specific surface characteristics.

This is an open access article under the terms of the [Creative Commons Attribution-NonCommercial](https://creativecommons.org/licenses/by-nc/4.0/) License, which permits use, distribution and reproduction in any medium, provided the original work is properly cited and is not used for commercial purposes.

© 2022 The Authors. *Clinical Oral Implants Research* published by John Wiley & Sons Ltd.

KEYWORDS

crestal bone formation, dehiscence type defects, implant geometry, implant surface, osseointegration

1 | INTRODUCTION

Osseointegrated dental implants have become a well-established modality for replacing missing teeth (Albrektsson et al., 1986). Technological improvements and increased patient demands have recently triggered a shift toward shorter and even immediate implant procedures (Buser et al., 2017). Likewise, the clinical outcome of dental implant procedures is not evaluated purely on functional requirements, but, increasingly, in terms of biological and esthetic considerations. (Choquet et al., 2001; Huang et al., 2021; Misch et al., 2008).

The anatomic parameters influencing immediate implant placement are well understood (Kan et al., 2011). Optimized osteotomy preparation techniques, geometrical implant designs, and surface modifications have been introduced to allow high primary and secondary stability (Javed et al., 2013; Puleo, 1999; Wilson et al., 2016).

Following implant placement and restoration, the crestal hard and soft tissues are subjected to ongoing changes (Albrektsson et al., 1986; Atsuta et al., 2016). Often, a gradual recession of the soft tissues around the implant, in conjunction with the resorption of supportive underlying crestal bone, can be observed (Atsuta et al., 2016). Consequently, high peri-implant crestal bone levels and a tight coronal soft tissue barrier have been proposed as critical for the long-term esthetic success of implant-supported restorations (Atsuta et al., 2016; Laurell & Lundgren, 2011).

Various implant designs and placement strategies have been introduced to achieve and maintain high crestal bone levels (Laurell & Lundgren, 2011; Valles et al., 2018). Changes in the surface roughness and hydrophilicity of the coronal aspect of the implant have, for example, been shown to effectively promote coronal bone growth and limit marginal bone loss, respectively (De Bruyn et al., 2017; Hermann et al., 2011; Schwarz et al., 2007). Subcrestally placed platform switched implants have also proven effective in limiting crestal bone loss (Valles et al., 2018). Recently, based on the hypothesis that marginal bone loss around rough implant surfaces might be higher, compared to machined or moderately rough implant surfaces (De Bruyn et al., 2017; Milleret et al., 2019; Susin et al., 2019), a new implant concept has been developed. Specifically, this implant concept is based on a novel gradient anodized (NGA) surface with a 2 mm zone, at the coronal implant collar, displaying minimal roughness (Milleret et al., 2019). Some controversy remains, however, regarding the effectiveness of this approach. Earlier clinical pilot studies, investigating subcrestal placement of implants with a smooth (either polished or machined) to rough transition, indicate that such configurations may not yield desirable results (Hämmerle et al., 1996; Hartman & Cochran, 2004).

Given the importance of high crestal bone levels for the biologic and esthetic success of dental implants, the present study aimed to

test the performance of NGA implants in comparison to implants modified with the established superhydrophilic moderately rough sandblasted acid-etched surface. The relative performance was investigated using a standardized buccal acute-type dehiscence model in minipigs, assessing crestal bone formation and osseointegration (Bosshardt et al., 2017; Rupp et al., 2006). Considering the potential influence of implant design on the osseointegration process, the study was designed to allow for distinguishing the relative contributions from surface characteristics and implant geometry.

2 | MATERIALS AND METHODS

2.1 | Study design

This controlled preclinical study aimed to investigate the influence of surface characteristics and implant geometry on their potential to promote crestal bone formation and osseointegration. The tested implants are schematically depicted in Figure 1a. In the following description, the three implant groups are designated by their group number followed by their role in the study. Moreover, information on the implant type, surface functionalization, base material, implant dimensions, and manufacturer is listed in parenthesis, for each implant group. The impact of surface characteristics was investigated by comparing (1, Test group) NGA functionalized, commercially available, implants (NobelActive, TiUltra NP, commercially pure Titanium, 3.5×8.5 mm, Nobel Biocare AG, Switzerland) with (2, Surface functionalization control group) custom-made replicas of the NGA implant geometry, modified with the SLActive surface (Replica of NobelActive, SLActive, Roxolid, 3.5 x 8.5 mm, Institut Straumann AG, Switzerland). Additionally, the potential influence on implant geometry was investigated by including (3, Implant geometry control group) a commercially available BLX implant (BLX, SLActive, Roxolid, 3.5 x 8 mm, Institut Straumann AG, Switzerland). All control implants were manufactured according to standard procedures for commercial implants (Institut Straumann AG, Switzerland).

De-novo crestal bone formation was analyzed histologically and histomorphometrically using a standardized acute type buccal dehiscence model after 2 and 8 weeks of healing. This model has previously proven effective for comparing implant surface modifications and was adopted in the mandible of minipigs for the current study (Schwarz et al., 2007, 2008).

A total of 15 Göttingen minipigs™, that is, 7 animals for the 2 weeks' time point and eight animals for the 8 weeks' time point, were included in the study. Study groups were compared by intra-animal comparison using one type of implant (group) per animal, for each study group. Implant positions were altered between animals by a rotation scheme, to ensure that each implant was represented

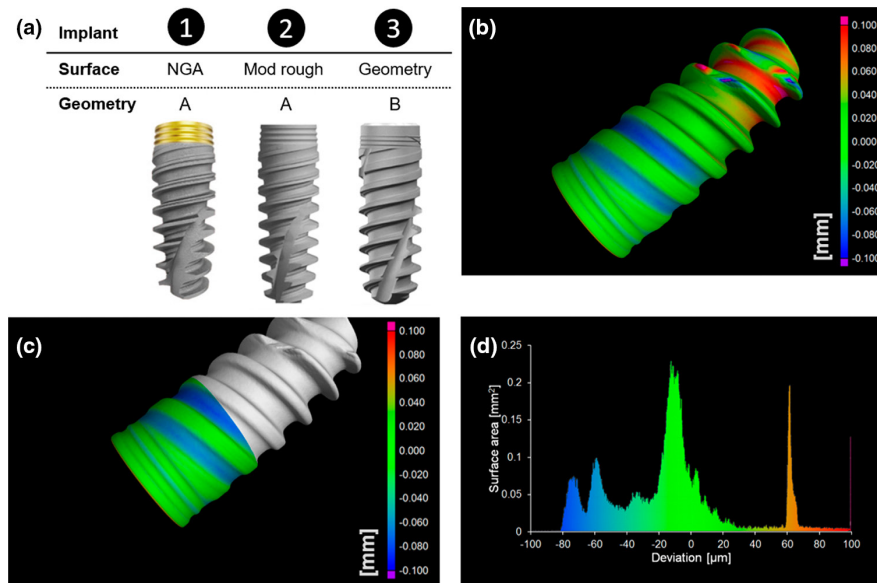


FIGURE 1 (a) Schematic illustration of study devices: NGA test implants (1), moderately rough control implant (2), geometry control implant (3). Implant 1 displays NGA surfaces. Implants 2 and 3 are functionalized to show a superhydrophilic, moderately rough, SLA-type surface. The geometric shape of implants of group 2 has been replicated from implant of group 1, that is, implants 1 and 2 display comparable geometrical shapes (geometry type a). Implant group 3 displays geometry type b. (b) Micro-computer tomography (μ CT) image with color-coded dimensional variations between NGA test (1) and moderately rough control implants (2), (c) μ CT image with color-coded dimensional variations between the same implants in the coronal region of interest. (d) Histogram of dimensional variations. Deviations corresponding to the peak at 60–70 μ m were detected primarily at the coronal platform and are related to implant length.

the maximum number of times at each anatomical position (left/right and mesial/distal) across the animals per healing period. Furthermore, due to the primary endpoint targeting the surface comparison and the geometry only as a secondary endpoint, care was taken to ensure Groups 1 and 2 were always placed on contralateral sides from one another. Each study group at the different healing periods had a $n = 6$ for the 2 weeks of healing and a $n = 8$ for the 8 weeks of healing. To reduce the number of animals used for research, each animal received three additional implant groups, that is, a total of 6 implants per animal that were part of a different study.

This study was conducted at the Biomedical Department of Lunds University (Lund, Sweden) and approved by the local Ethics Committee of the University (M-192-14) following the proper institutional and national guidelines for the care and use of the animals in the study. This study adhered to the ARRIVE 2.0 Guidelines and was designed by considering the 3R principle for animal research (Percie du Sert et al., 2020).

2.2 | Replication of NGA test implants and characterization of moderately rough control implants

Implants of groups 1 and 2 were scanned using microCT (Zeiss Metrotom 1500 G3, Zeiss, Germany) with a voltage of 15 kV, a current of 100 μ A, and an averaging time of 2000 ms from a flat part position and a resolution of 0.015 mm. The raw data files were converted into CAD/CAM format using the program Design X (v2020.0, 3D System). Implant blanks were milled of TiZr and subsequently

surface-modified as described above according to standard procedures (Institut Straumann AG).

Implants of groups 1 and 2 were compared in terms of microCT scan overlays (VGStudio Max, v3.4.5, Volume Graphics) (Figure 1), scanning electron microscopy (Figure 2), surface roughness measurements, and dynamic contact angle measurements (DCA) (Table 1).

Surface analyses were carried out as previously described (Pippenger et al., 2019). In brief, advancing contact angles were measured by the dynamic Wilhelmy method on a KRÜSS K100 tensiometer (Krüss GmbH) in deionized water. Surface roughness was assessed using a μ surf explorer confocal microscope and μ softAnalysisXT software (NanoFocus AG) at 20 \times magnification. Surface parameters were evaluated on 798 \times 798 μ m² using a Gaussian wavelength cutoff of 50 \times 50 μ m². Surface roughness was quantified in S_a values, as defined by the average height deviation from the mean plane.

Surface morphology was evaluated using a Zeiss Supra 55 SEM (Carl Zeiss AG) equipped with an Everhart-Thornley secondary electron detector at high and low acceleration voltages of 15 and 5 kV, respectively. Surface characteristics were determined as triplicates and are reported as mean values.

2.3 | Animals

Fifteen female Göttingen Minipigs™ (Ellegaard) of age between 20–24 months at the time of surgery and an average body weight of

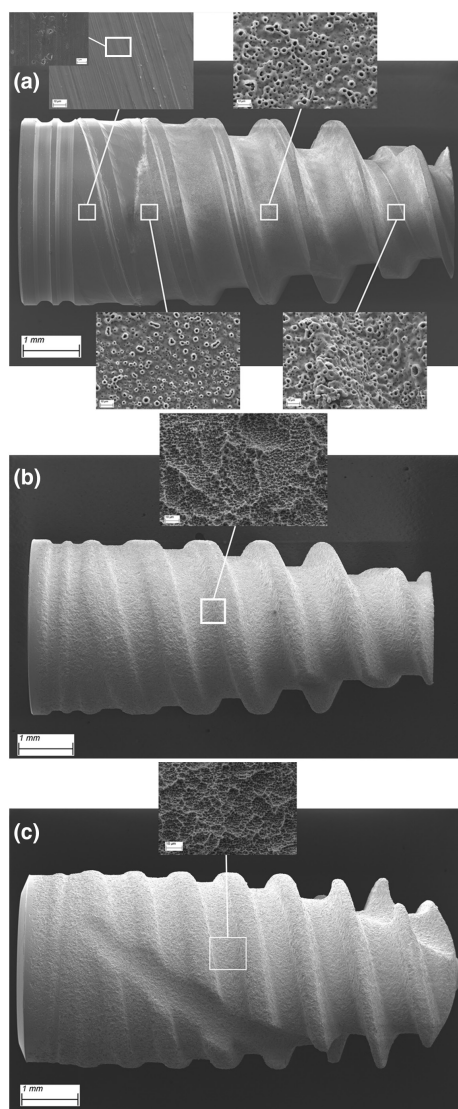


FIGURE 2 Overview scanning electron micrograph and zoomed regions of interest (insertions) of implant group 1 (a); 4 ROIs; coronal ROI with a second ROI insertion at a higher magnification, 2 (b; 1 ROI zoom), and 3 (c; 1 ROI insertion). Bars in main images: 1 mm, bars in insertions: 10 μ m, bar in second insertion for the coronal section of the group 1 implant: 1 μ m

40 kg were included in the study. The animals were housed in standard boxes in groups of three. Animals were adapted to experimental conditions by starting animal housing 1 week before intervention. Animals were fed a standard soft food diet (Special Diet Services [SDS], Witham, UK #801586). Animals were fasted overnight before surgery, to prevent vomiting.

2.4 | Surgical procedure

All surgical procedures were performed under general anesthesia using a combination of dexmedetomidine (25–35 μ g/kg i.m., Dexdomitor; Orion Pharma Animal Health) and tiletamine-zolazepam (50–70 mg/kg i.m., Zoletil 100 Vet, Virbac) injected intramuscularly

and maintained with intravenous infusion after induction with propofol (PropoVet multidose, Orion Pharma Animal Health) and fentanyl (Fentanyl B. Braun). Carprofen (4 mg/kg, s.i.d., i.m., Rimadyl vet., Orion Pharma Animal Health) was given as a preemptive dose and post-surgically up to 4 days together with buprenorphine (0.03 mg/kg, i.m., Vetergesic vet, Orion Pharma Animal Health). To reduce the dosage of the systemic anesthetic, bleeding during surgery, and to alleviate post-surgical pain, local anesthesia was provided intraoperatively by infiltrative injection of 1.8 ml of Xylocaine (Xylocaine, Dental adrenalin, 20 mg/ml and 12.5 μ g/ml; Astra AB) per hemi-mandible.

Antibiotic prophylaxis was administered using benzylpenicillin-prokain-dihydrostreptomycin (25 mg/kg + 20 mg/kg, s.i.d., i.m., Streptocillin vet., Boehringer Ingelheim Vetmedica). Animals were intubated and breathing withheld by a ventilator. Vital parameters were monitored continuously (pulse oximetry, rectal temperature, blood pressure, CO₂).

2.5 | Tooth extraction

Three contralateral mandibular premolars (P2–P4) and first mandibular molars (M1) were carefully extracted using a minimally invasive surgical approach, that is, without raising a flap.

2.6 | Implant osteotomy and buccal dehiscence defect preparation and implant placement

Implants were placed 20 weeks' post-extraction. As depicted in Figure 3, mandibular alveolar ridges were exposed by elevation of a mucoperiosteal flap after midcrestal incision and flattened using a cylindrical cutting bur under saline irrigation. Implant positions for the test and control implants were rotated between left/right and the P3, P4, and M1 positions.

Implant osteotomies were prepared according to the manufacturer's instructions, using the corresponding drills and drill sequences. In brief, osteotomies for groups 1 and 2 were prepared as per manufacturer's guidelines for hard bone, using the sequence: $\varnothing 2.0 \rightarrow \varnothing 2.4/2.8 \rightarrow \varnothing 2.8/3.2 \rightarrow$ Tap Drill (Nobel Twist and Step drills, Nobel Biocare AG). Osteotomies for group 3 were prepared as per manufacturer's guidelines for hard bone, using a sequence: $\varnothing 2.2 \rightarrow \varnothing 3.2 \rightarrow \varnothing 3.5$ (only coronal 4 mm) (VeloDrill, Institut Straumann AG). Following osteotomy preparation, buccal dehiscence-type defects (3 \times 3 \times 3 mm) were created with a Lindemann drill as previously described (Figure S2B) (Schwarz et al., 2008). Briefly, after ridge flattening and osteotomy preparation, a dental probe was used to measure 3 mm in depth from the edge of the ridge. A Lindemann drill (Diameter \varnothing 0.1 mm; L 9.0 mm) was then used to drill perpendicularly into the buccal wall through to the implant osteotomy. This was repeated for the neighboring side of the defect. Then, the edge of the Lindemann was used to cut across, connecting the two drill holes with a through cut. Finally, downward cuts were performed (apical direction) from the ridge down to the original drill holes.

TABLE 1 Comparison of surface roughness values and wettability properties of the study implants as stratified by region of interest along the implant long axis

Implant group	Property	Coronal position			
		Collar 1–2 mm	Transition 3 mm	Middle 4–5 mm	Apex 7 mm
1	$S_a \pm SD$ (μm)	0.662 ± 0.176	0.680 ± 0.079	1.079 ± 0.240	1.617 ± 0.208
	CA	$0 \pm 0^\circ$			
2	$S_a \pm SD$ (μm)	1.206 ± 0.078			
	CA	$0 \pm 0^\circ$			
3	$S_a \pm SD$ (μm)	1.315 ± 0.021			
	CA	$0 \pm 0^\circ$			

Note: N = 3.

Abbreviations: CA, advancing water contact angle; S_a , arithmetic means of the surface points from the mean plane; SD, standard deviation.

Implants were placed at crestal level using a motorized hand-piece followed by a custom-made torque ratchet (Institut Straumann AG). Primary implant stabilities were assessed in terms of maximum insertion torques (max IT).

Implants were subsequently equipped with closure screws and covered by porcine collagen membrane (Geistlich Bio-Gide, Geistlich) followed by primary wound closure (Vicryl® 5.0, Ethicon) for submerged healing. Antibiotic cover and optional analgesia, as described above, were administered for 7 days post-surgery (Streptocilin vet, Boehringer Ingelheim, 3–4 ml/pig i.m.).

2.7 | Termination

Animals were sacrificed by intra-cardiac injection of a 20% solution of pentobarbital (Pentobarbitalnatrium, Apoteket AB; 60 mg/ml).

Block sections of the implant sites were prepared with an oscillating autopsy saw under perseveration of the soft tissues and fixed in formalin (4% formaldehyde solution) for at least 2 weeks before histological processing.

2.8 | Histological processing

Formalin-treated block sections were dehydrated using ascending grades of alcohol and xylene and, subsequently, infiltrated and embedded in methyl methacrylate (MMA, Sigma Aldrich; Polymerized by Perkadox 16, Nouryon) for non-decalcified sectioning. Block sections were then cut in a buccolingual direction to sections of 500 μm (EXAKT Systems, Germany)(1 central section per implant) and ground to a final thickness of 30–50 μm . Sections were stained with paragon (toluidine blue and basic fuchsin) for microscopic evaluation.

2.9 | Quantitative histomorphometry

Histomorphometric parameters were evaluated on central buccolingual sections of the implant and exclusively on the buccal aspects of

the implant (the buccal aspect comprised the defect site). The evaluated histomorphometric parameters are illustrated in Figure S1.

The primary outcome of this study was crestal bone formation. The histomorphometric parameter directly associated with this outcome was as follows:

- New bone height (NBH) as defined by the maximum height of the newly formed bone crest in the defect (Figure S1A)

Secondary outcomes were related to the capacity of the individual implant surfaces to promote osseointegration and bone apposition and included the following:

- The percentage of bone-to-implant contact in the dehiscence defect area (dBIC) (Figure S1C, ROI 1)
- Vertical bone creep (VBC) as defined by the height of newly formed bone within the defect area in direct contact with the implant (Figure S1D)
- First bone-to-implant contact (fBIC) as calculated by the distance between the implant shoulder and the most coronal aspect of bone in direct contact to the implant (Figure S1E)
- Bone area to total area (BATA) as the ratio between the area occupied by newly formed bone and the total defect area (Figure S1B)

Further, the capacity of the implants to promote osseointegration was evaluated by assessing the bone-to-implant contact in apical native bone (ROI 2) (nBIC) (See Figure S1F).

2.10 | Statistical evaluation

Adjusted histomorphometric parameters, 95% confidence intervals (CI), and associations to the different test items under consideration of the factor mandible side and position, in the mandible, were calculated individually for the 2 and 8 weeks' time points using mixed linear regression models (Tables S1 and S2). The adjusted means and the 95% confidence intervals extracted from the models are reported throughout the manuscript.

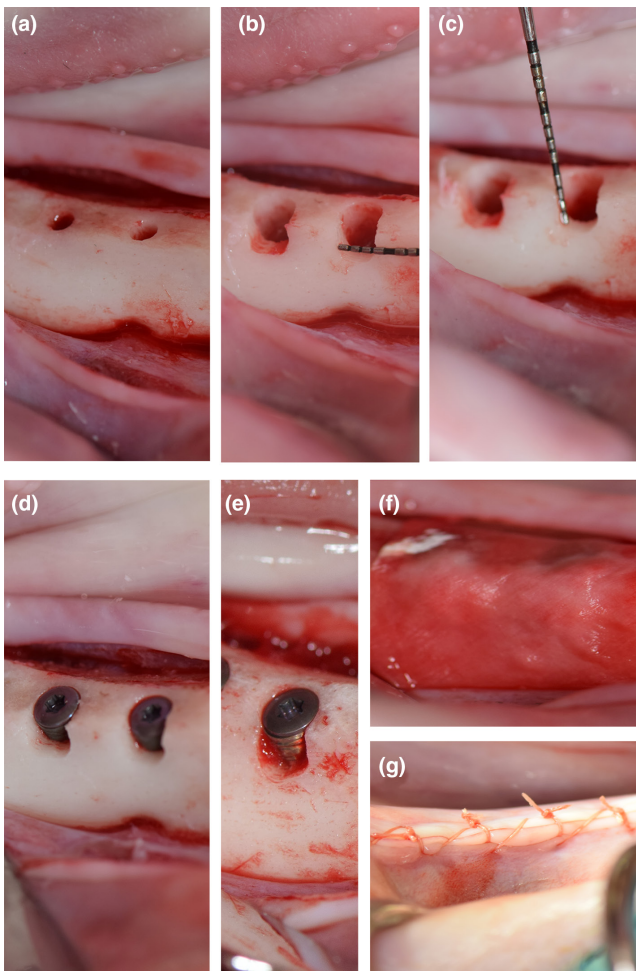


FIGURE 3 Illustration of individual steps of the surgical procedure. (a) Implant osteotomy preparation starting from a flattened mandibular alveolar ridge. (b, c) creation of standardized acute-type buccal dehiscence type defect ($3 \times 3 \times 3$ mm). (d, e) implant placement at crestal level (in panel d, the left implant is group 2; the right implant is group 3; in panel e, the implant represented is group 1). (f) Coverage with a collagen membrane. (g) Primary wound closure

The correlation between histomorphometric outcomes and the implant geometry, implant surface, and the factors, healing time, mandible side, and mandible position were also derived from mixed linear regression models (Table S3). Both models included the factor “animal” as a random effect. The Dunnett-Hsu method was used to adjust for multiple comparisons. The unit of analysis was the subject (animal), and the significance level was set to an $\alpha < .05$. The software SAS version 9.4 (2016, SAS Institute Inc., Cary) was used for the analysis. The complete set of results from the statistical models is provided as part of supplementary information. The power of the study was calculated post hoc using the obtained parameters at week 8 and setting the level to 0.05 for a two-tailed paired test.

3 | RESULTS

3.1 | Implant geometry comparisons between NGA test implants and geometric replicas and surface characterization

To ensure comparable implant geometries of groups 1 and 2, specifically at the coronal aspect of the implant, interfacing the acute-type dehiscence defect, the three-dimensional implant geometries of both implants were compared by microCT. As evidenced by the 3D overlays in Figure 1b, differences were detected and these were most pronounced in the apical portion of the implants. Specifically, the threads of group 1 were found to be approximately $100 \mu\text{m}$ deeper, compared to group 2, at the apical region. Deviations in the coronal part of the implants were less pronounced, with group 2 showing slightly deeper threads (blue zones in Figure 1c) and a marginally higher coronal platform (orange zones in Figure 1c). The histogram in Figure 1d illustrates that these deviations ranged from -80 to $-60 \mu\text{m}$ in the threads and $+60$ to $+70 \mu\text{m}$ for the coronal platform height, respectively.

Figure 2 and Table 1 further compare and illustrate the characteristics and parameters related to implant surface topographies, surface roughness, and wettability. Scanning electron microscopy (SEM) images and surface roughness measurements of group 1 revealed four zones with changing surface topographies and different S_a values. Specifically, the coronal aspect of group 1 displayed a 2 mm wide zone with a relatively smooth pore-free surface, showing striations and groves and with a relatively low S_a value of $0.662 \pm 0.176 \mu\text{m}$. Group 1 displayed increasingly pronounced volcano-shaped features, and an associated increase in surface roughness parameters, moving in the apical direction. Specifically, S_a values ranged from $0.680 \pm 0.079 \mu\text{m}$, at the first transition zone, 3–4 mm from the coronal platform to $1.617 \pm 0.208 \mu\text{m}$ at the implant apex. SEM images of groups 2 and 3 revealed a homogenous surface topography displaying micro-sized features at two predominant length scales, that is, periodic pits of diameters between 1–2 μm and 10–50 μm , respectively. The S_a values of groups 2 and 3 were $1.206 \pm 0.078 \mu\text{m}$ and $1.315 \pm 0.021 \mu\text{m}$, respectively. All implants displayed superhydrophilic characteristics with advancing contact angles of $0 \pm 0^\circ$ (Table 1).

3.2 | In-vivo investigation

3.2.1 | Animal response to implantation and primary stability assessments

All animals recovered from surgery in a predictable manner and without any intra- or post-surgical complications. One of the animals sacrificed at the 2 weeks' time point displayed an osteoporotic phenotype as identified during histological processing, characterized by

a very thin amount of crestal mandibular bone and a correspondingly large medullary cavity. The resultant histometric measurements were found to be outliers and were thus excluded from the analysis, resulting in 6 and 8 implants per test group for the 2 and 8 weeks' time points, respectively.

All implants displayed appropriate and comparable primary stability as evidenced by insertion torque value measurements for individual time points or averaged over both time points (1: 48.3 ± 24.7 Ncm, 2: 38.0 ± 26.1 Ncm, and 3: 35.1 ± 24.8 Nm).

Figure 4 compares the histological cross-sections focusing on the buccal dehiscence defects between study groups, after 2 and 8 weeks of healing. All implants healed well and osseointegrated without any signs of fibrous encapsulation. Healing after 2 weeks was characterized by the formation of a provisional matrix and trabecular primary woven bone that formed starting from the apical margin of the defect. After 8 weeks, the dehiscence defects showed an advanced healing stage, characterized by mature lamellar bone and a widely healed bone crest around all implants. Qualitative differences regarding crestal height and quantity were apparent, with groups 2 and 3 displaying a similar increased crestal height and amount of newly formed bone compared to group 1. These surface type-associated differences were further analyzed by histology, comparing the detailed healing patterns for groups 1 and 2 at higher magnification.

As evidenced by the histological micrographs in Figure 5, distinct qualitative differences in the buccal dehiscence defect

healing patterns, around groups 1 and 2, were identified at both healing time points. Specifically, after 2 weeks, differences were related to the degree of mineralization of newly formed bone and the quantity of direct bone apposition to the implant surface (Figure 5a). At the 8 weeks' time point, differences were mainly related to direct bone apposition and the newly formed bone crest (Figure 5b).

After 2 weeks, the healing for group 1 was characterized by new trabecular bone of relatively low mineralization. Interestingly, direct contacts between the newly formed bone matrix and the implant surface were widely absent. By contrast, group 2 showed pronounced bone apposition of newly formed bone in direct contact with the implant surface. Also, the newly formed bone, seen for group 2, appeared distinctly more mature when compared to group 1, based on the ratio between mineralized, frank bone matrix and osteoid, being higher for group 2 than for group 1.

After 8 weeks of healing, the morphology of crestal bone associated with group 1 displayed a wedge-shaped defect-like morphology around the implant surface. This defect-like morphology transitioned into a detectable slit-like gap between the newly formed bone and the implant surface, in an apical direction. Group 2, by contrast, displayed a horizontal bone crest with mature lamellar bone in direct contact with the implant surface and ongoing crestal osteoid formation at the implant surface.

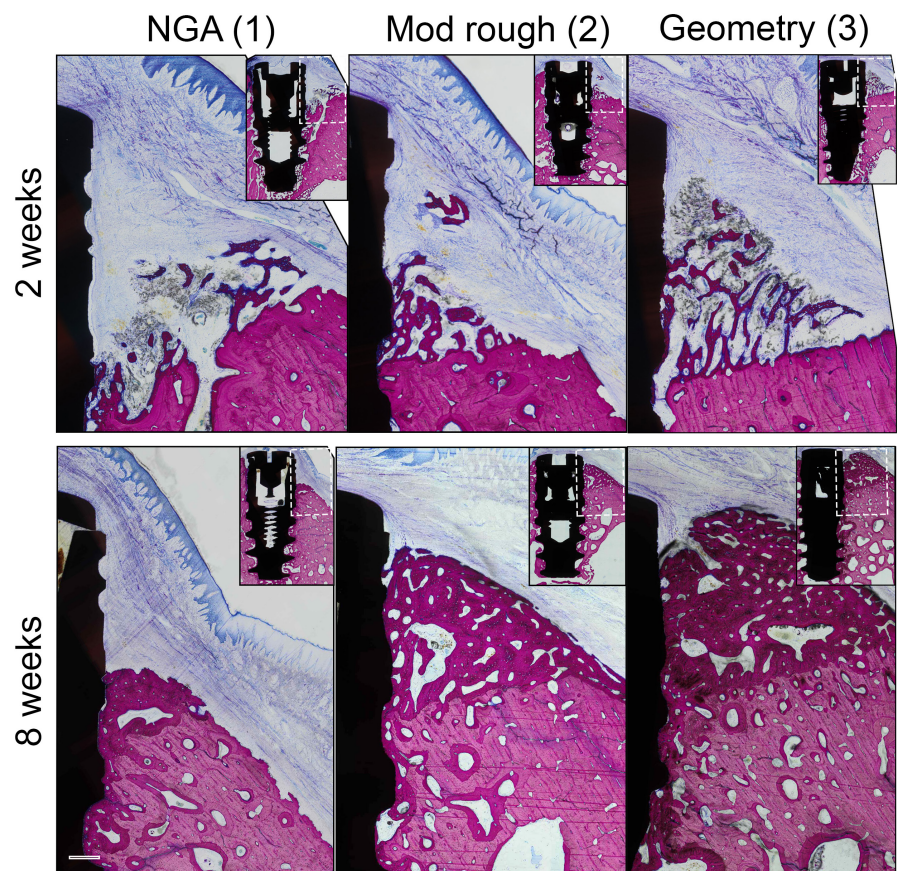


FIGURE 4 Representative micrographs of histological cross-sections comparing the healing pattern and de-novo crestal bone formation in acute-type dehiscence defects around NGA test implants (1), moderately rough control implants (2), and geometry control implants (3) after 2 weeks (upper row) and 8 weeks of healing (lower row). Insertions show the histological overviews. Scale bar = 1 mm

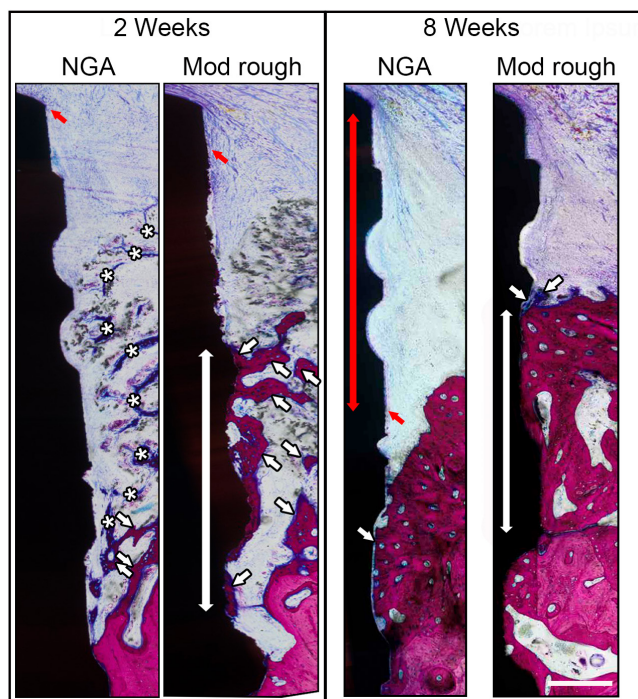


FIGURE 5 Representative histological cross-sections of acute-type dehiscence defects at higher magnification comparing the healing pattern in proximity to NGA and moderately rough implant surfaces of groups 1 and 2 after 2 weeks (a) and 8 weeks (b) of healing. (a) 2 weeks of healing: Asterisks denote trabeculae of newly forming bone (osteoid). This early and premature bone type was predominant around implants of group 1. White arrows indicate early trabecular frank mineralized bone lined by osteoid seams. This more mature bone type appeared dominant around implants of group 2. The white double arrow marks the length of the implant surface in contact with newly formed bone (from within the original defect area). Bone apposition to moderately rough surfaces was more pronounced as compared to NGA surfaces. (b) 8 weeks of healing: NGA implant surfaces were characterized by a wedge-like gap at the coronal aspect of the dehiscence defect that transitioned into a thin non-mineralized slit-like gap, interposed between the implant surface and newly formed lamellar bone in the apical direction (white arrow). The small red arrow and double arrow mark the extent of epithelial downgrowth detected at the coronal aspects of the implant surface and the extent of the zone in which this epithelium was apparent, respectively. Moderately rough implant surfaces were characterized by mature lamellar bone in direct contact with the implant surface (white double arrow). Small white arrows mark osteoid at the crestal aspects of newly formed bone. Scale bar = 500µm

3.2.2 | Histomorphometry

The height and amount of newly formed crestal bone in the dehiscence defect, as a function of group, were histomorphometrically compared after 2 and 8 weeks of healing in terms of NBH and BATA. VBC, fBIC, and dBIC were further assessed to interpret crestal bone formation in the context of bone apposition to the implant surface and implant osseointegration. Additionally, the groups were compared in terms of implant osseointegration in native apical bone

(nBIC). Differences between the 2 and 8 weeks' time points were consistent but more pronounced at the 8 weeks' time point.

Crestal bone height after 8 weeks, as assessed by NBH, was observed to be significantly higher for group 3 implants (mean 2116µm, 95% CI: 1638–2595µm) when compared to group 1 implants (mean 1683µm, 95% CI: 1204–2162µm) ($p = .0225$). The amount of newly formed crestal bone as evaluated in terms of BATA after 8 weeks of healing was also highest for group 3 (mean 74.30%, 95% CI: 65.69%–82.82%) and group 2 (66.80%, 95% CI: 58.18%–75.42%), compared to group 1 (mean 55.45%, 95% CI: 46.83%–64.07%). Both differences reached statistical significance ($p = .0029$ and $p = .0492$, respectively) (Figure 6a,b).

Bone apposition and osseointegration as assessed in terms of dBIC (Figure 6c), VBC (Figure 6d), and fBIC (Figure 6e) at the 8 weeks' time point were consistently and significantly higher for groups 2 and 3, compared to group 1. Specifically, group 2 (mean 35.95%, 95% CI: 26.36%–45.54%) and group 3 (mean 34.90%, 95% CI: 25.30%–44.49%) showed significantly higher osseointegration in terms of dBIC, compared to group 1 (mean 7.22%, 95% CI: 2.37%–16.81%) ($p = .0005$ and $p = .0007$ respectively). Also, after 8 weeks, groups 2 and 3 showed significantly higher crestal bone formation at the implant surface in terms of VBC, that is, 2 (mean 1519µm, 95% CI: 1043–1995µm) and 3 (mean 1500µm, 95% CI: 1025–1976µm), compared to group 1 (mean 803µm, 95% CI: 328–1279µm) ($p = 0.0029$ and $p = .0038$, respectively). fBIC for groups 2 and 3 was also significantly higher, when compared to group 1, that is, 3 (mean -719µm, 95% CI: -1126 to -312µm) and 2 (mean -716µm, 95% CI: -1122 to -308µm), compared to group 1 (mean -1772µm, 95% CI: -2179 to -1365µm) ($p = .0005$ and $p = .0004$, respectively).

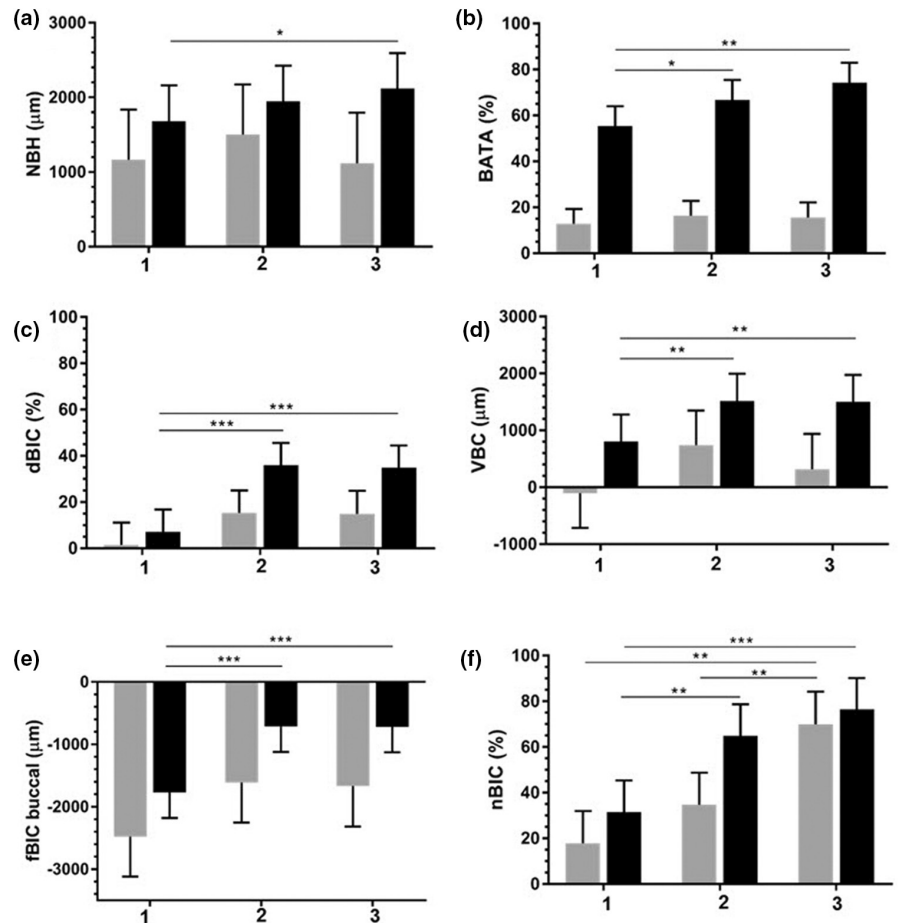
The osseointegration for groups 2 and 3, in native bone (nBIC) (Figure 6f), was again significantly higher after 8 weeks of healing compared to group 1, that is, 2 (mean 64.92%, 95% CI: 51.13%–78.71%) and 3 (mean 76.46%, 95% CI: 62.69%–90.25%), compared to 1 (mean 31.57%, 95% CI: 17.79%–45.36%) ($p = .0048$ and $p = .0007$, respectively). Interestingly, nBIC after 2 weeks was significantly higher for group 3 when compared to group 1 ($p = .0011$) and 2 ($p = .0083$). It may be emphasized that nBIC after 2 weeks was the only parameter and timepoint that showed a strong and significant influence of implant geometry, when comparing groups 2 and 3.

The power of the study to test the null hypothesis of no difference in NBH between implants 1 and 2 (different surfaces and same geometry) was calculated post hoc. The mean study difference between implant 2 and 1 of -263.02 ± 220.16 mm in NBH (Table S2) was used and the alpha level was set to .05 for a two-tailed paired test. With 8 pairs (subjects), the power of the study is 0.825.

3.3 | Influence of study variables on crestal bone formation, osseointegration, and bone apposition

A mixed linear regression model was further used to analyze the influence of surface modification and implant geometry on crestal bone formation and osseointegration (Figure S2, Table S3). This model

FIGURE 6 Comparison of histomorphometric parameters between different implant groups after 2 and 8 weeks of healing: (a) NBH, New crestal bone height; (b) BATA, Ratio of bone area to total area in the defect (ROI 1); (c) dBIC, Bone-to-implant contact in the dehiscence defect area (ROI 1); (d) VBC, Vertical bone creep; (e) fBIC, First bone-to-implant contact; (f) nBIC, Native bone to implant contact in the apical region of interest (ROI 2). Individual values represent adjusted mean values by mixed linear regression. Error bars designate the 95% confidence intervals. Levels of significance as adjusted according to Dunnett-Hsu: * $p \leq .05$, ** $p \leq .01$, *** $p \leq .001$



indicated that the surface type significantly affected all histological parameters related to crestal bone formation and osseointegration, except for NBH. Specifically, the model resulted in consistently higher adjusted BATA, dBIC, VBC, and fBIC values for moderately rough implants compared to NGA implants. Interestingly, the bone-to-implant contact in native bone (nBIC) was the only parameter affected by both implant geometry and surface type, resulting in higher values for the implant geometry of group 3, compared to the implant geometries of groups 1 and 2. NBH revealed no clear association to either geometry or surface type. All histomorphometric parameters increased with healing time, a majority of which were significant.

4 | DISCUSSION

This study investigated the influence of implant surface properties and implant geometry on crestal bone formation in acute-type dehiscence defects and on the osseointegration in native bone. The impact of implant surface properties was examined for two superhydrophilic surface types, that is, the novel gradient anodized surfaces (NGA, group 1) and the large-grit sandblasted and acid-etched surface (Moderately rough, group 2), having the same implant geometry. Additionally, the impact of implant geometry was evaluated using a second tapered implant geometry, also with the moderately rough surface (group 3).

From the comparison of the different study groups, the following main observations were obtained: (A) Although NBH was found to be greater for group 1 after 2 and 8 weeks, these differences were not statistically different. Likewise, there were no statistical differences in NBH between groups 2 and 3. The only statistical difference was observed at 8 weeks between groups 1 and 3, with a bigger NBH for group 3. We conclude that the surface properties alone cannot fully account for the differences seen in NBH. (B) All remaining defect-related variables (BATA, dBIC, VBC, and fBIC) were superior for implant groups 2 and 3 at 8 weeks of healing, and thus, differences may be associated with surface properties. (C) Osseointegration in native bone (nBIC) was found to be associated with implant surface properties and the implant geometry. The effect of implant geometry was statistically significant (1 vs. 3) at the 2 weeks' time point. At the 8 weeks' time point, the surface characteristics were found to have the largest impact on nBIC, as no significant difference was observed between groups 2 and 3, while both groups showed significant higher values compared to group 1.

The influence of implant characteristics on osseointegration has been thoroughly investigated in previous studies. Modification of surface properties, that is, roughness, wettability, surface energy, implant material, or implant geometry, has all been shown to strongly influence the process of osseointegration (Ogle, 2015; Rupp et al., 2006; Smeets et al., 2016; Wilson et al., 2016). The implant geometries, utilized for the current study, were selected so that groups 1 and 2 had the same geometry. Group 3 had a

different geometry but was also functionalized with the moderately rough surface, as was the case for group 2.

Considering that group 2 was a replica of group 1, some degree of variation is to be expected. The comparison of the implants from groups 1 and 2 showed minor deviations, and these were mainly localized to the bottom region of the implant threads. Specifically, the threaded region at the coronal part of the implant showed slightly deeper threads, compared to the original. At the apical part, the threads of the replica were found to be shallower, compared to the reference. Keeping in mind the dimensional scale at which the histomorphometric parameters were assessed, and the magnitude of the variations between groups, for the assessed parameters the potential impact of the dimensional differences between groups 1 and 2 are considered marginal and, therefore, to have a negligible impact on the study outcome.

Since groups 2 and 3 showed similar performances, for BATA, dBIC, VBC, and fBIC, the results strongly indicate that the superior crestal bone formation observed for groups 2 and 3, compared to group 1, predominantly arises from differences in surface structures and/or chemistry and are less influenced by the different geometry represented by group 3.

Schwarz et al. (Schwarz et al., 2007, 2008) have previously compared the de novo crestal bone formation around titanium implants as a function of surface hydrophilicity in a standardized canine buccal dehiscence type model. Here, the authors found that crestal bone formation around hydrophilic SLA active surfaces was enhanced, compared to hydrophobic SLA surfaces (Schwarz et al., 2007). Immunohistological follow-up studies revealed that this enhanced bone formation was associated with the particular ability of the SLA active surface to stabilize the blood clot, which was essential for the subsequent formation of a well-organized preliminary collagen-rich matrix. On the other hand, less hydrophilic surfaces led to a collapse of the blood clot at the implant surface, which impeded bone formation. Considering that all test groups of the current study show superhydrophilic surface characteristics, the observed differences cannot be contributed to the mechanisms described by Schwarz et al. Schwarz et al., 2007, 2008. and, thus, must be contributed to either surface structure or chemistry.

The design of the acute-type dehiscence defect model infers that the surface structures presented by the gradient design of group 1 will change as a function of the distance from the coronal aspect, going from relatively smooth toward moderately rough at the apical region. For the current model, the relatively smooth neck of the implant will be exposed to the defect as compared to the moderately rough surface of groups 2 and 3, where the roughness parameters remain the same, along the length of the implant. As a result, the work by Di Iorio et al., where the extent of fibrin clot extension as a function of surface roughness was investigated, could potentially hint toward the mechanism behind the observations of the current study, relating to the defect site. The authors reported that rough implant surfaces, compared to smooth machined implant surfaces, displayed a significantly increased tendency to promote a more extensive and three-dimensional complex blood clot (Di Iorio et al., 2005). Based on these previous reports, we hypothesize that differences in crestal bone formation between the moderately rough and NGA surfaces, observed herein, may have

been associated with similar effects and differences in the ability of the surfaces to promote blood clot adhesion. The importance of implant surface roughness for crestal bone formation might also be indicated by the observation that group 1 implants lacked bone apposition, to the coronal aspect, at the early healing time point. This resulted in the formation of wedge-shaped to slit-like defects between the bone and the implant surface, at the late healing time point. Further, the apical position of the smooth to moderately rough transition of NGA implants (2mm subcoronal) appear to match with the crestal level of newly formed bone after 8 weeks of healing, indicating that bone formation around NGA implants was limited toward the coronal direction by the presence of the smooth zone at the coronal implant aspect. This is further supported by the study of Botticelli et al. (Botticelli et al., 2005) examining the healing of marginal defects, around turned and SLA-modified dental implants, in a canine model. Here, inferior defect healing and BIC% was observed for the turned implants.

Analyzing the results of the current study in the light of the findings by Di Iorio et al., Botticelli et al., and Schwarz et al., it appears that the effects of superhydrophilicity are not sufficient to ensure optimal osseointegration in the absence of roughness. However, considering the results for nBIC, roughness alone does not appear to be the sole factor at play. This is the case since inferior performance of group 1 is also observed for the nBIC parameter, measured from the middle to the apical aspect of the implant. Here, the roughness of the NGA surface is found to range from S_a 1.079 ± 0.240 (middle) to 1.617 ± 0.208 (apex) μm , compared to the uniform roughness of S_a $1.206 \pm 0.078 \mu\text{m}$ for the moderately rough surface of group 2. Hence, both surfaces predominantly present moderately rough surface features for ROI 2. Looking at the SEM images presented in Figure 3, it is evident that a comparison of the two surfaces by means of a single roughness parameter is not sufficient. The work by Wennerberg and Albrektsson summarizes the complexity of surface roughness of dental implants and, further, sheds light on this by also addressing the roughness at the nanometer range (Wennerberg & Albrektsson, 2009, 2010). Such, in-depth, characterization of the different groups has been outside the scope of the current work, however, it would be interesting to further examine the aspects of surface structures and chemistry that might contribute to understanding the current findings.

Concerning the applied animal model, Schwarz et al. (Schwarz et al., 2008) reported that acute-type crestal defects displayed a certain tendency to spontaneously heal by bone formation originating from open marrow spaces at the lateral aspects of the defect. A similar self-healing effect might be observed in the porcine model used for the current study as, despite consistently higher histomorphometric parameters related to bone apposition and osseointegration around moderately rough surfaces, the model failed to clearly show differences in new bone height between groups 2 and 1. This aspect may be considered a potential limitation of the applied model when evaluating the results related to new crestal bone height.

Besides crestal bone formation, this study also investigated osseointegration in native bone as a function of implant geometry and surface modifications. Interestingly, implant geometry type B (group 3) displayed superior osseointegration at the 2 weeks' time point, while the geometry type A (groups 1 and 2) was only capable of

achieving comparable levels of nBIC, at the 8 weeks' time point, when modified with the moderately rough surface. These results illustrate the importance of surface properties to promote osseointegration. They also illustrate that both implant surface and geometry impact synergistically the osseointegration process. Another potential contribution to the observed difference at the 2 weeks' time point could be the fact that different implant geometries imply differences in osteotomy preparation. Even though insertion torque values and, thus, the indirect primary stability of the test groups was comparable, a potential positive effect of a shorter drill protocols on the osseointegration for group 3 might not be entirely excluded (Heuzeroth et al.).

As noted above, both investigated technologies displayed superhydrophilic properties, however, these properties were maintained by two different routes. The superhydrophilic properties of the moderately rough surfaces are maintained by wet storage (groups 2 and 3) while the NGA (group 1) surface is maintained by a protective salt layer (Lüers et al., 2016; Milleret et al., 2019; Rupp et al., 2006). The differences in storage condition also represent a difference in the surface chemistry; hence, this might be a factor contributing to the observed differences. Finally, minor differences between the tested implants were related to the implant material (cpTi vs. TiZr). Previous studies failed to show a significant difference in osseointegration between these material types (Saulacic et al., 2012; Gottlow et al., 2012). The effects observed in the current study may, therefore, not be related to the differences in implant materials.

Finally, certain limitations associated with this study should be noted. Overall, these results were obtained within an animal model. As porcine and human bone have been reported to have similar anatomical and healing characteristics, the results of this study indicate that osseointegration may develop similarly in a clinical setting. In terms of groups, in order to more clearly separate the influences of the surface and the geometry, a BLX implant with the NGA surface would have needed to be included as a fourth group. Due to the logistical limitation of producing such a group, any conclusions on the implant geometry must remain suggestive in nature. Finally, the defects were created in as standardized a manner as possible. Anatomical differences between animals result in differing buccal thicknesses and thus more or less injured bone to contribute to the regenerative process. However, this was mitigated by allocating groups equally across anatomical positions and by performing the study with a statistically acceptable number of animals. The statistical power of the current study was determined post hoc based on previous experience with similar studies performed using the present animal model.

5 | CONCLUSION

The extent of de novo crestal bone formation in acute-type dehiscence defects appears to be primarily influenced by implant surface characteristics and was in line with the ability of the individual implant surface to promote osseointegration and direct bone apposition.

The potential of the apical, endosteal implant aspects to osseointegrate was influenced by a combination of surface properties

and geometry. At early healing time points, implant geometry modifications can significantly affect endosteal osseointegration and may outperform the effect of surface modifications.

AUTHOR CONTRIBUTIONS

Shakeel Shahdad: Conceptualization (equal); data curation (equal); formal analysis (equal); funding acquisition (equal); investigation (equal); methodology (equal); resources (equal); validation (equal); writing – review and editing (equal). **Dieter D Bosshardt:** Data curation (equal); formal analysis (equal); resources (equal); writing – review and editing (equal). **Mital Patel:** Conceptualization (equal); data curation (equal); formal analysis (equal); resources (equal); writing – review and editing (equal). **Nahal Razaghi:** Conceptualization (equal); formal analysis (equal); methodology (equal); resources (equal); validation (equal); writing – original draft (equal). **Anuya Patankar:** Formal analysis (equal); investigation (equal); resources (equal); writing – review and editing (equal). **Mario Rocuzzo:** Conceptualization (equal); data curation (equal); funding acquisition (equal); methodology (equal); project administration (equal); resources (equal); validation (equal); writing – review and editing (equal).

ACKNOWLEDGMENTS

The author would like to thank Leticia Grize for the statistical analysis and Novonexile AG (Switzerland) for writing assistance and editorial support in preparing the manuscript.

CONFLICT OF INTEREST

The present study was funded by a grant from Institut Straumann AG. SS and MR receive speaker honorariums for educational courses from Institut Straumann AG. DB, MP, NR, and AP declare no conflict of interest.

DATA AVAILABILITY STATEMENT

The data that support the findings of this study are available from the corresponding author upon reasonable request.

ORCID

Shakeel Shahdad  <https://orcid.org/0000-0001-5354-9847>

Mario Rocuzzo  <https://orcid.org/0000-0002-2135-6503>

REFERENCES

- Albrektsson, T., Zarb, G., Worthington, P., & Eriksson, A. R. (1986). The long-term efficacy of currently used dental implants: A review and proposed criteria of success. *The International Journal of Oral & Maxillofacial Implants*, 1, 11–25.
- Atsuta, I., Ayukawa, Y., Kondo, R., Oshiro, W., Matsuura, Y., Furuhashi, A., Tsukiyama, Y., & Koyano, K. (2016). Soft tissue sealing around dental implants based on histological interpretation. *Journal of Prosthodontic Research*, 60, 3–11.
- Bosshardt, D. D., Chappuis, V., & Buser, D. (2017). Osseointegration of titanium, titanium alloy and zirconia dental implants: Current knowledge and open questions. *Periodontology* 2000, 73, 22–40.
- Botticelli, D., Berglundh, T., Persson, L. G., & Lindhe, J. (2005). Bone regeneration at implants with turned or rough surfaces in self-contained defects. An experimental study in the dog. *Journal of Clinical Periodontology*, 32, 448–455.

- Buser, D., Chappuis, V., Belsler, U. C., & Chen, S. (2017). Implant placement post extraction in esthetic single tooth sites: When immediate, when early, when late? *Periodontology* 2000, 73, 84–102.
- Choquet, V., Hermans, M., Adriaenssens, P., Daelemans, P., Tarnow, D. P., & Malevez, C. (2001). Clinical and radiographic evaluation of the papilla level adjacent to single-tooth dental implants. A retrospective study in the maxillary anterior region. *Journal of Periodontology*, 72, 1364–1371.
- De Bruyn, H., Christiaens, V., Doornewaard, R., Jacobsson, M., Cosyn, J., Jacquet, W., & Vervaeke, S. (2017). Implant surface roughness and patient factors on long-term peri-implant bone loss. *Periodontology* 2000, 73, 218–227.
- Di Iorio, D., Traini, T., Degidi, M., Caputi, S., Neugebauer, J., & Piattelli, A. (2005). Quantitative evaluation of the fibrin clot extension on different implant surfaces: An in vitro study. *Journal of Biomedical Materials Research Part B: Applied Biomaterials*, 74, 636–642.
- Gottlow, J., Dard, M., Kjellson, F., Obrecht, M., & Sennerby, L. (2004). Evaluation of a new titanium-zirconium dental implant: a biomechanical and histological comparative study in the mini pig. *Clin Implant Dent Relat Res*, 14(4), 538–45.
- Hämmerle, C. H., Brägger, U., Bürgin, W., & Lang, N. P. (1996). The effect of subcrestal placement of the polished surface of ITI implants on marginal soft and hard tissues. *Clinical Oral Implants Research*, 7, 111–119.
- Hartman, G. A., & Cochran, D. L. (2004). Initial implant position determines the magnitude of crestal bone remodeling. *Journal of Periodontology*, 75, 572–577.
- Hermann, J. S., Jones, A. A., Bakaeen, L. G., Buser, D., Schoolfield, J. D., & Cochran, D. L. (2011). Influence of a machined collar on crestal bone changes around titanium implants: A histometric study in the canine mandible. *Journal of Periodontology*, 82, 1329–1338.
- Huang, X., Bai, J., Liu, X., Meng, Z., Shang, Y., Jiao, T., Chen, G., & Deng, J. (2021). Scientometric analysis of dental implant research over the past 10 years and future research trends. *BioMed Research International*, 2021, 1–13.
- Javed, F., Ahmed, H. B., Crespi, R., & Romanos, G. E. (2013). Role of primary stability for successful osseointegration of dental implants: Factors of influence and evaluation. *Interventional Medicine and Applied Science*, 5, 162–167.
- Kan, J. Y. K., Roe, P., Rungcharassaeng, K., Patel, R. D., Waki, T., Lozada, J. L., & Zimmerman, G. (2011). Classification of sagittal root position in relation to the anterior maxillary osseous housing for immediate implant placement: A cone beam computed tomography study. *The International Journal of Oral & Maxillofacial Implants*, 26(4), 873–876.
- Laurell, L., & Lundgren, D. (2011). Marginal bone level changes at dental implants after 5 years in function: A meta-analysis: Marginal bone level changes at dental implants. *Clinical Implant Dentistry and Related Research*, 13, 19–28.
- Lüers, S., Laub, M., & Jennissen, H. P. (2016). Protecting ultra- and hyperhydrophilic implant surfaces in dry state from loss of wettability. *Current Directions in Biomedical Engineering*, 2, 557–560.
- Milleret, V., Lienemann, P. S., Gasser, A., Bauer, S., Ehrbar, M., & Wennerberg, A. (2019). Rational design and in vitro characterization of novel dental implant and abutment surfaces for balancing clinical and biological needs. *Clinical Implant Dentistry and Related Research*, 21, 15–24.
- Misch, C. E., Perel, M. L., Wang, H.-L., Sammartino, G., Galindo-Moreno, P., Trisi, P., Steigmann, M., Rebaudi, A., Palti, A., Pikos, M. A., Schwartz-Arad, D., Choukroun, J., Gutierrez-Perez, J.-L., Marenzi, G., & Valavanis, D. K. (2008). Implant success, survival, and failure: The international congress of Oral Implantologists (ICOI) Pisa Consensus conference. *Implant Dentistry*, 17, 5–15.
- Ogle, O. E. (2015). Implant surface material, design, and osseointegration. *Dental Clinics of North America*, 59, 505–520.
- Percie du Sert, N., Hurst, V., Ahluwalia, A., Alam, S., Avey, M. T., Baker, M., Browne, W. J., Clark, A., Cuthill, I. C., Dirnagl, U., Emerson, M., Garner, P., Holgate, S. T., Howells, D. W., Karp, N. A., Lázic, S. E., Lidster, K., MacCallum, C. J., Macleod, M., ... Würbel, H. (2020). The ARRIVE guidelines 2.0: Updated guidelines for reporting animal research. *PLoS Biology*, 18(7), e3000410.
- Pippenger, B. E., Rottmar, M., Kopf, B. S., Stübinger, S., Dalla Torre, F. H., Berner, S., & Maniura-Weber, K. (2019). Surface modification of ultrafine-grained titanium: Influence on mechanical properties, cytocompatibility, and osseointegration potential. *Clinical Oral Implants Research*, 30, 99–110.
- Puleo, D. (1999). Understanding and controlling the bone-implant interface. *Biomaterials*, 20, 2311–2321.
- Rupp, F., Scheideler, L., Olshanska, N., de Wild, M., Wieland, M., & Geisgerstorfer, J. (2006). Enhancing surface free energy and hydrophilicity through chemical modification of microstructured titanium implant surfaces. *Journal of Biomedical Materials Research. Part A*, 76, 323–334.
- Saulacic, N., Bosshardt, D. D., Bornstein, M. M., Berner, S., & Buser, D. (2012). Bone apposition to a titanium-zirconium alloy implant, as compared to two other titanium-containing implants. *Eur Cell Mater*, 10(23), 273–286.
- Schwarz, F., Herten, M., Sager, M., Wieland, M., Dard, M., & Becker, J. (2007). Bone regeneration in dehiscence-type defects at chemically modified (SLActive) and conventional SLA titanium implants: A pilot study in dogs. *Journal of Clinical Periodontology*, 34, 78–86.
- Schwarz, F., Rothamel, D., Herten, M., Wüstefeld, M., Sager, M., Ferrari, D., & Becker, J. (2008). Immunohistochemical characterization of guided bone regeneration at a dehiscence-type defect using different barrier membranes: An experimental study in dogs. *Clinical Oral Implants Research*, 19, 402–415.
- Smeets, R., Stadlinger, B., Schwarz, F., Beck-Broichsitter, B., Jung, O., Precht, C., Kloss, F., Gröbe, A., Heiland, M., & Ebker, T. (2016). Impact of dental implant surface modifications on osseointegration. *BioMed Research International*, 2016, 1–16.
- Susin, C., Finger Stadler, A., Musskopf, M. L., Sousa Rabelo, M., Ramos, U. D., & Fiorini, T. (2019). Safety and efficacy of a novel, gradually anodized dental implant surface: A study in Yucatan mini pigs. *Clinical Implant Dentistry and Related Research*, 21, 44–54.
- Valles, C., Rodríguez-Ciurana, X., Clementini, M., Baglivo, M., Paniagua, B., & Nart, J. (2018). Influence of subcrestal implant placement compared with eucristal position on the peri-implant hard and soft tissues around platform-switched implants: A systematic review and meta-analysis. *Clinical Oral Investigations*, 22, 555–570.
- Wennerberg, A., & Albrektsson, T. (2009). Effects of titanium surface topography on bone integration: A systematic review. *Clinical Oral Implants Research*, 20, 172–184.
- Wennerberg, A., & Albrektsson, T. (2010). On implant surfaces: A review of current knowledge and opinions. *The International Journal of Oral & Maxillofacial Implants*, 25, 63–74.
- Wilson, T. G., Miller, R. J., Trushkowsky, R., & Dard, M. (2016). Tapered implants in dentistry: Revitalizing concepts with technology: A review. *Advances in Dental Research*, 28, 4–9.

SUPPORTING INFORMATION

Additional supporting information can be found online in the Supporting Information section at the end of this article.

How to cite this article: Shahdad, S., Bosshardt, D., Patel, M., Razaghi, N., Patankar, A., & Rocuzzo, M. (2022). Benchmark performance of anodized vs. sandblasted implant surfaces in an acute dehiscence type defect animal model. *Clinical Oral Implants Research*, 33, 1135–1146. <https://doi.org/10.1111/clr.13996>